Open access • Journal Article • DOI:10.1103/PHYSREVB.100.125141

Magnetization, d -wave superconductivity, and non-Fermi-liquid behavior in a crossover from dispersive to flat bands — Source link

Pramod Kumar, Päivi Törmä, Tuomas I. Vanhala

Institutions: Ludwig Maximilian University of Munich

Published on: 18 Sep 2019 - Physical Review B (American Physical Society)

Topics: Hubbard model, Mean field theory, Fermi liquid theory, Square lattice and High-temperature superconductivity

Kumar, Pramod; Torma, Paivi; Vanhala, Tuomas

Magnetization, d-wave superconductivity, and non-Fermi-liquid behavior in a crossover from dispersive to flat bands

Published in:
Physical Review B

DOI:
10.1103/PhysRevB.100.125141

Published: 18/09/2019

Document Version
Publisher's PDF, also known as Version of record

Please cite the original version:
Kumar, P., Torma, P., & Vanhala, T. (2019). Magnetization, d-wave superconductivity, and non-Fermi-liquid behavior in a crossover from dispersive to flat bands. *Physical Review B*, *100*(12), 1-11. [125141]. https://doi.org/10.1103/PhysRevB.100.125141

Magnetization, *d*-wave superconductivity, and non-Fermi-liquid behavior in a crossover from dispersive to flat bands

Pramod Kumar and Päivi Törmä
Department of Applied Physics, Aalto University, Helsinki, 00076 Aalto, Finland

Tuomas I. Vanhala
Department of Physics, Arnold Sommerfeld Center for Theoretical Physics (ASC), Munich Center for Quantum Science and Technology (MCQST), Fakultät für Physik, Ludwig-Maximilians-Universität München, D-80333 München, Germany

(Received 20 March 2019; revised manuscript received 9 September 2019; published 18 September 2019)

We explore the effect of inhomogeneity on electronic properties of the two-dimensional Hubbard model on a square lattice using dynamical mean-field theory (DMFT). The inhomogeneity is introduced via modulated lattice hopping such that in the extreme inhomogeneous limit the resulting geometry is a Lieb lattice, which exhibits a flat-band dispersion. The crossover can be observed in the uniform sublattice magnetization which is zero in the homogeneous case and increases with the inhomogeneity. Studying the spatially resolved frequency-dependent local self-energy, we find a crossover from Fermi-liquid to non-Fermi-liquid behavior happening at a moderate value of the inhomogeneity. This emergence of a non-Fermi liquid is concomitant of a quasiflat band. For finite doping the system with small inhomogeneity displays *d*-wave superconductivity coexisting with incommensurate spin-density order, inferred from the presence of oscillatory DMFT solutions. The *d*-wave superconductivity gets suppressed for moderate to large inhomogeneity for any finite doping while the incommensurate spin-density order still exists.

DOI: 10.1103/PhysRevB.100.125141

I. INTRODUCTION

In his famous 1989 paper [1], Lieb considered Hubbard models on certain bipartite lattices with highly degenerate single-particle states, which he showed to have ground states with nonzero spin. Magnetism in such flat-band models has later been the subject of many theoretical and computational studies [2–9]. Another type of order studied in connection with flat bands is superconductivity, where electronic pairing can be enhanced by the high density of states [10–13]. While flat-band models such as the Lieb lattice were originally intended as theoretical toy models, developments in experimental techniques in ultracold gases and condensed matter systems now allow them to be created and studied. A striking example of how flat bands can enhance correlation effects is twisted bilayer graphene [14–16], where certain "magic" twist angles lead to superconductivity and insulating states whose precise nature is not yet understood. Flat-band systems have also been engineered by manipulating the electronic surface states of a copper crystal using adsorbed molecules [17–19] and using optical potentials for bosonic [19–21] and fermionic [22] ultracold quantum gases. The advantage of these experiments is the high degree of tunability in the lattice parameters.

In both electronic and optical lattice experiments, the most commonly used flat-band model system is the Lieb lattice [19], whose simple structure makes it relatively easy to be implemented. However, because of experimental imperfections, exactly flat bands are difficult to achieve. This motivates us to introduce a model, pictured in Fig. 1, that is an interpolation between the Lieb lattice and the simple square lattice, and exhibits a band with a *tunable* bandwidth. This can also be compared to twisted bilayer graphene where the width of the low-energy bands can be tuned by changing the twist angle [23]. A related idea, where suitably chosen next-nearest-neighbor hoppings lead to partially flat bands and typical flat-band effects such as enhanced superconducting transition temperatures and non-Fermi-liquid behavior, has been studied in recent works [24,25]. A π-flux lattice model [26] exhibiting Dirac fermions with a tunable velocity has also been considered. Our main goal here is to study the crossover between the flat-band physics and normal dispersive behavior, allowing us to build a general picture of how flat-band effects on magnetic states would be observed in experiments. Interestingly, the model also provides a new perspective to flat-band ferromagnetism on the Lieb lattice: We find that the ground state as a whole is always antiferromagnetic with no total magnetic moment. However, as the model is tuned toward the Lieb-lattice limit, a subset of the lattice sites carrying a magnetic moment becomes weakly coupled to the rest of the lattice. Thermal fluctuations easily reduce the magnetization of the weakly coupled part, thus leading to a total magnetization that *increases* with temperature.

Another motivation for our work is to study how the *d*-wave superconducting states of the square-lattice model [27] interact with the flat band. While the general idea is that flat bands can boost interaction effects by decreasing the competition from kinetic energy, leading to strong correlations and high critical temperatures for ordered states, this is not the whole story: For ordered states resulting from strong correlation effects beyond the mean-field level, the single-particle band structure may be rather irrelevant. In fact,

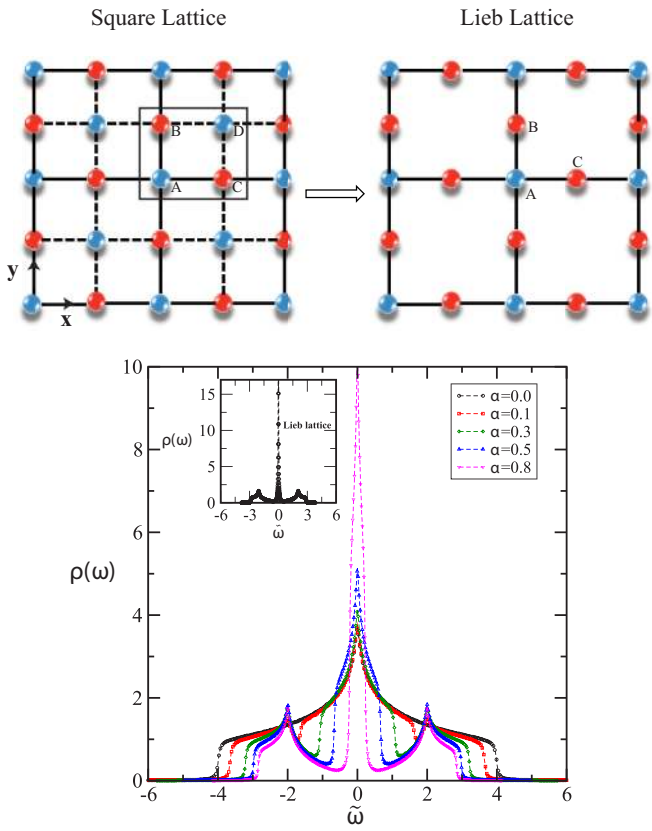

FIG. 1. Upper panel: schematic representation of the inhomogeneity introduced by modulated hopping. The solid lines represent the hopping amplitude $(1+\alpha)t$, while the dashed lines represent $(1-\alpha)t$. The square drawn by the solid line is the smallest possible unit cell that captures magnetic and superconducting order parameters emerging at finite Hubbard interaction. In the limit $\alpha = 1$, the square lattice with modulated hopping turns into the Lieb lattice. Lower panel: the noninteracting density of states (DOS) of the inhomogeneous lattice as a function of the normalized energy parameter $\tilde{\omega}$ (see text) for different choices of α. The density of states evolves from square-lattice behavior to Lieb-lattice one. In the inset: DOS for the pure Lieb lattice.

we show that the d-wave superconductivity is monotonically suppressed as the model is tuned toward the Lieb-lattice limit, which is apparently because the asymmetry between the A and D sites is incompatible with the local, correlated mechanism leading to the d-wave pairing. In this context, the model is best seen as a type of *inhomogeneous* square-lattice model, meaning a model where the hopping amplitudes or onsite potentials can vary spatially. Motivation for such models is related to the so-called stripe order, i.e., spatially nonuniform spin-density or charge-density order, which has been found in several families of the cuprates [28,29] and also in ultracold atom experiments recently [30], albeit only in one-dimensional (1D) systems. Other examples of inhomogeneity include quasiperiodic systems [31], fermionic ultracold atoms in harmonic traps [32], electron systems on surfaces [33], interfaces [34], and topological insulating systems [35,36].

Whether the presence of incommensurate spin and density order competes with or helps the emergence of superconductivity (SC) in real materials is in general unsettled [37,38]. Theoretical studies report both suppression and enhancement of d-wave superconductivity (dSC) order with inhomogeneity [39–44], depending on the inhomogeneity pattern and strength, interaction strength, and doping of the system. A much studied inhomogeneity pattern is the 2D Hubbard model on a checkerboard lattice where the strong and weak nearest-neighbor hopping amplitudes alternate along both directions [41,43–46]. A stripe version of the model, where the nearest-neighbor hopping amplitude is modulated along one direction, has also been considered [43]. Other inhomogeneity patterns are checkerboardlike and stripelike variations in the local onsite potential on 2×2 plaquettes [39]. To study the inhomogeneous square-lattice Hubbard model introduced here, we employ dynamical mean-field theory (DMFT) and its cluster extensions. In Sec. II, we introduce the model as an interpolation between the square and the Lieb lattices, followed by the formalism of real-space DMFT to capture spatially resolved local order parameters and cellular DMFT that can capture the nonlocal correlations essential to dSC. In Secs. III A and III B, we discuss the effect of the inhomogeneity and the quasiflat band on the emergent magnetic order and the double occupancy, respectively. The breakdown of the Fermi-liquid behavior in the crossover from dispersive to flat-band behavior is discussed in Sec. III C. Finally, we discuss the effect of the inhomogeneity on the behavior of dSC and incommensurate spin- and density-wave order in Sec. III D.

II. MODEL AND METHOD

The grand canonical Hamiltonian of the Hubbard model for an inhomogeneous square lattice as shown in Fig. 1(a) can be expressed as $H = H_t - \mu N + H_U$, where the first term is the tight-binding part represented in standard second quantized notation as

$$H_t = -\sum_{\langle ij\rangle,\sigma} [(t_{ij} c^\dagger_{i,\sigma} c_{j,\sigma} + \text{H.c.})], \tag{1}$$

where $c^\dagger_{j,\sigma}$ is the creation operator corresponding to different sites of the unit cell at $j = (x, y)$ and σ labels spin. We have introduced the inhomogeneity via the modulated next-nearest hopping by setting $t_x = t[1 + (-1)^y \alpha]$ and $t_y = t[1 + (-1)^x \alpha]$, where $\alpha = 0$ corresponds to the homogeneous square lattice and $\alpha = 1$ represents the Lieb lattice as shown in Fig. 1. The Lieb lattice resembles the CuO_2 planes of the high-T_c cuprate superconductors with blue (red) circles representing copper (oxygen) ions [12]. However, there is a huge onsite energy difference between the copper and oxygen orbitals, violating one of the criteria of Lieb's theorem [1]. Additionally, the ground state of the cuprates is aniferromagnetic unlike the ferromagnetic ground state of the Lieb lattice. The second term μN of the full Hamiltonian introduces the chemical potential, where the total particle number is $N = \sum_{j,\sigma} c^\dagger_{j,\sigma} c_{j,\sigma}$.

The last term is the onsite Hubbard interaction which can be defined as

$$H_U = U \sum_j \left(n_{j,\uparrow} - \frac{1}{2}\right)\left(n_{j,\downarrow} - \frac{1}{2}\right), \tag{2}$$

where U is the interaction strength with $U > 0$ for the repulsive Hubbard model. To account for the aforementioned inhomogeneity, the smallest possible unit cell has four sites as shown by the solid square in Fig. 1. The tight-binding Hamiltonian in momentum space can be written as

$$H_{\rm t} = \sum_{k,\sigma} \psi^{\dagger}_{\mathbf{k}\sigma} H_{\rm t}(\mathbf{k}) \psi_{\mathbf{k}\sigma},$$

where $\psi_{\mathbf{k}\sigma} = (c_{A\sigma}\ c_{B\sigma}\ c_{C\sigma}\ c_{D\sigma})^T$ and

$$H_t(\mathbf{k}) = -2\begin{pmatrix} 0 & t_+\cos k_x & t_+\cos k_y & 0 \\ t_+\cos k_x & 0 & 0 & t_-\cos k_y \\ t_+\cos k_y & 0 & 0 & t_-\cos k_x \\ 0 & t_-\cos k_y & t_-\cos k_x & 0 \end{pmatrix}$$

with $t_\pm = (1 \pm \alpha)t$. The energy eigenvalues of the tight-binding Hamiltonian can be given as

$$E_{\mathbf{k}} = \pm 2t\sqrt{(1+\alpha^2)S_+ \pm \sqrt{(1+\alpha^2)^2 S_+^2 - (1-\alpha^2)^2 S_-^2}}, \tag{3}$$

where $S_+ = \cos^2 k_x + \cos^2 k_y$ and $S_- = \cos^2 k_x - \cos^2 k_y$. For $\alpha = 1$, the resulting geometry is the Lieb lattice with $E_{\mathbf{k}} = 0$ and $E_{\mathbf{k}} = \pm 2\sqrt{2}t\sqrt{\cos^2 k_x + \cos^2 k_y}$. In the lower panel of Fig. 1, we show the DOS vs $\tilde{\omega}$, where $\tilde{\omega} = \omega/t(1+\alpha)$, for the tight-binding part of the Hamiltonian for different choices of α. The DOS has a Van Hove singularity at zero energy for $\alpha = 0$, which grows with increasing inhomogeneity parameter α into a narrow peak structure, ultimately turning into a δ function representing the flat band of the Lieb lattice for $\alpha = 1$ (see inset of Fig. 1).

To investigate the effects of correlations and inhomogeneity at half-filling, we have employed real-space dynamical mean-field theory (RDMFT) [47,48] for finite Hubbard interactions. DMFT maps a lattice problem into an effective single-impurity problem taking into account the lattice effects in a self-consistent manner [49]. Within single-site DMFT the self-energy $\Sigma_{ij\sigma}(i\omega_n)$ is assumed to be spatially local and uniform, so that $\Sigma_{ij\sigma}(i\omega_n) \sim \delta_{ij}\Sigma_\sigma(i\omega_n)$. The i and j are the lattice site indices, $\omega_n = \pi(2n+1)T$, where T is the temperature, are the Matsubara frequencies, and σ is the spin index. For the inhomogeneous case, however, the uniformity assumption is relaxed. Hence, we use RDMFT where the self-energy is still local but varies spatially, i.e., $\Sigma_{ij\sigma}(i\omega_n) = \Sigma^i_\sigma(i\omega_n)\delta_{ij}$ [47].

The RDMFT method for a given unit cell can be described as follows. The local Green's function of the lattice system can be calculated as

$$\mathbf{G}_\sigma(i\omega_n) = \frac{1}{N_{\mathbf{k}}}\sum_{\mathbf{k}} \left(\mathbf{G}^0_{\mathbf{k}\sigma}(i\omega_n)^{-1} - \mathbf{\Sigma}_\sigma(i\omega_n)\right)^{-1}, \tag{4}$$

where the bold quantities are matrices of the dimension 4×4 and $N_{\mathbf{k}}$ is the number of $\mathbf{k}$ points. Thus, the matrix element $\mathbf{G}_\sigma(i\omega_n)_{ij}$ is the Green's function between sites i and j of the unit cell. The noninteracting Green's function $\mathbf{G}^0_{\mathbf{k}\sigma}(i\omega_n)^{-1} = \mu_\sigma + i\omega_n - \mathbf{T}_{\mathbf{k}}$, where $\mathbf{T}_{\mathbf{k}}$ is the superlattice Fourier transform of the hopping matrix. The self-energy is assumed to be diagonal in the site indices. For each site i in the unit cell, there is an effective single-impurity Anderson model, which is defined by the dynamical Weiss mean field

$$\mathcal{G}^i_\sigma(i\omega_n)^{-1} = (\mathbf{G}_\sigma(i\omega_n)_{ii})^{-1} + \Sigma^i_\sigma(i\omega_n)_{ii}. \tag{5}$$

Using the Weiss function $\mathcal{G}^i_\sigma$, we calculate the self-energy of each of the impurity problems using an impurity solver. These new self-energies are supplied again to Eq. (4) and the process is iterated to find a converged solution.

We use exact diagonalization (ED) and continuous-time quantum Monte Carlo (CT-INT) as impurity solvers at zero temperature and finite temperature, respectively. [27,50]. We define the local magnetization $m_i = n_{i,\uparrow} - n_{i,\downarrow}$, where $n_{i,\sigma} = G_{i,\sigma}(\tau \to 0^-)$ is the density of spin-σ particles for a given site of the unit cell. Another important quantity to measure the effects of correlation is the double occupancy $D = \langle n_{i,\uparrow} n_{i,\downarrow}\rangle$, representing the tendency of two particles to occupy the same site. It is 0.25 in the zero interaction limit while it vanishes in the Mott insulating large-U limit for the repulsive Hubbard model for a homogeneous system at half-filling. It can be directly calculated using DMFT+CT-INT as

$$D = \frac{n_i}{2} - \frac{\langle k\rangle_{\rm MC}}{\beta|U|} - \frac{1}{4}, \tag{6}$$

where $n_i = n_{i,\uparrow} + n_{i,\downarrow} = 1$ for half-filling and $k_{\rm MC}$ is the Monte Carlo perturbation order [50]. Additionally, the double occupancy for a site can be directly compared with the local moment m_i^2 measured in the experiments [51], given as

$$\langle m_i^2\rangle = 1 - 2\langle n_{i\uparrow} n_{i\downarrow}\rangle. \tag{7}$$

To study superconductivity within DMFT, we use the Nambu formalism [42,52], where the Green's function can be written in the Nambu-spinor notation as

$$G_{ij}(\tau) = -\langle \mathcal{T}\psi_i(\tau)\psi^{\dagger}_j(0)\rangle, \tag{8}$$

where $\psi_i(\tau) \equiv (c_{i\uparrow}, c^{\dagger}_{i\downarrow})^T$ and its matrix notation can be given as

$$\mathbf{G}(\tau) = \begin{pmatrix} \mathbf{G}_\sigma(\tau) & \mathbf{F}(\tau) \\ \mathbf{F}^{\dagger}(\tau) & -\mathbf{G}_{\bar{\sigma}}(-\tau) \end{pmatrix},$$

where τ is imaginary time, and $G_{ij\sigma}(\tau) \equiv -\langle \mathcal{T}c_{i\sigma}(\tau)c^{\dagger}_{j\sigma}(0)\rangle$ and $F_{ij}(\tau) \equiv -\langle \mathcal{T}c_{i\downarrow}(\tau)c_{j\uparrow}(0)\rangle$ are the normal and anomalous Green's functions, respectively. To capture a nonlocal dSC order parameter, emerging away from half-filling, we employ cellular dynamical mean field theory (CDMFT). Within CDMFT, a lattice problem is mapped to a finite cluster coupled to a noninteracting bath. In our case the cluster is a four-site 2×2 plaquette as shown in Fig. 1, which has been used to study the dSC order in the canonical square-lattice Hubbard model [27,53,54]. The local cluster Green's function of the lattice system is given by the matrix equation

$$\mathbf{G}_c(i\omega_n) = \frac{1}{N_{\mathbf{k}}}\sum_{\mathbf{k}} (\mathbf{G}^0(\mathbf{k}, i\omega_n)^{-1} - \mathbf{\Sigma}_c(i\omega_n))^{-1}, \tag{9}$$

where $N_{\mathbf{k}}$ is the number of $\mathbf{k}$ points. The noninteracting Green's function $\mathbf{G}^0(\mathbf{k}, i\omega_n)^{-1} = i\omega_n + \mu\sigma_z - \mathbf{T}(\mathbf{k})\sigma_z$, where $\mathbf{T}_{\mathbf{k}}$ is the superlattice Fourier transform of the hopping matrix with dimension equal to the number of sites in the cluster, i.e., 4×4. The cluster self-energy $\mathbf{\Sigma}_c(i\omega_n)$ can be given as

$$\mathbf{\Sigma}_c(i\omega_n) = \begin{pmatrix} \mathbf{\Sigma}_\uparrow(i\omega_n) & \mathbf{S}(i\omega_n) \\ \mathbf{S}(i\omega_n) & -\mathbf{\Sigma}^*_\downarrow(i\omega_n) \end{pmatrix},$$

where $\Sigma_{ij\sigma}(i\omega_n)$ $[S_{ij}(i\omega_n)]$ is the normal (anomalous) part of the self-energy matrix of dimension 4×4.

Similar to the the single-site DMFT, there is an effective impurity problem for the cluster, which can be defined by the Weiss mean field

$$\mathcal{G}_c^0(i\omega_n)^{-1} = \mathbf{G}_c^{-1}(i\omega_n) + \mathbf{\Sigma}_c(i\omega_n). \tag{10}$$

This quantity is also known as the "bath function" and represents the noninteracting Green's function of the impurity problem. Given the mean field $\mathcal{G}_c^0$, we calculate the cluster propagator and the self-energy $\Sigma_c(i\omega_n)$ from the above Weiss mean field using ED as an impurity solver [27]. The process is iterated similar to single-site DMFT to find the solution. We define the average magnetization for the cluster as

$$m_{\text{avg}} = \sum_i \frac{|m_i|}{4}, \tag{11}$$

where m_i is the local magnetization of a given site calculated from the normal Green's function. Additionally, we can define the average dSC order for the given four-site cluster as

$$\Delta_{\text{avg}} = \frac{\Delta_{AB} + \Delta_{BD} + \Delta_{DC} + \Delta_{CA}}{4}, \tag{12}$$

$\Delta_{ij} = S_{ij}(\langle c_{i\downarrow} c_{j\uparrow}\rangle - \langle c_{i\uparrow} c_{j\downarrow}\rangle)/2$ with $\langle c_{i\downarrow} c_{j\uparrow}\rangle = F_{ij}(\tau \to 0^-)$ and $F_{ij}(\tau)$ is the nonlocal anomalous Green's function of the unit cell. For the singlet $d_{x^2-y^2}$ pairing on a square lattice we have

$$S_{ij} = \begin{cases} 1 \text{ if } i-j = \pm\hat{x}, \\ -1 \text{ if } i-j = \pm\hat{y}, \end{cases}$$

where $\hat{x}$ and $\hat{y}$ are unit lattice vectors.

III. RESULTS

In this section, we discuss the effect of the inhomogeneity and Hubbard interaction for two cases: (1) half-filling, where number of particles per site is one, and (2) away from half-filling with finite doping $x = 1 - n_{\text{avg}}$, where $n_{\text{avg}} = \sum_i \frac{n_i}{4}$ is the average density over the unit cell. At half-filling, the interplay of inhomogeneity and interaction is visible in the local magnetism and the double occupancy. One of the key purposes of this work is to study the quasiparticle behavior in the inhomogeneous system. We calculate the local self-energy and show breakdown of Fermi-liquid behavior with increasing strength of the inhomogeneity. The result that we find can be associated to the (quasi)flat band present in the inhomogeneous system. Away from half-filling, we present a phase diagram as a function of inhomogeneity α and chemical potential μ, showing $\Delta(\mu, \alpha)$ at $U = 6.0$. We also show the averaged magnetic order m_{avg} for different set of μ and α. The dSC order parameter decreases with α and vanishes further for moderate to large α. The magnetic order coexists with dSC for small values of α. For a moderately inhomogeneous system, incommensurate magnetic order is present with no dSC.

A. Magnetism

Due to the spatial inhomogeneity introduced by the modulated hoppings, the local magnetic order is nonuniform across different sites. We show the spatially resolved magnetic order m evaluated using ED+RDMFT at zero temperature for varying interaction strength $\tilde{U} = U/t_+$ at different α in Fig. 2. We allow the breaking of the SU(2) spin-rotation symmetry to capture the magnetically ordered state. An initial self-energy that is constant in the Matsubara frequency is added in way that it breaks SU(2) symmetery of the Hamiltonian. For a homogeneous system, i.e., $\alpha = 0$, local magnetic order gradually develops with finite Hubbard interactions such that $m_A = -m_{B/C} = m_D$ for any $\tilde{U} > 0$. For weak interaction, the behavior of the magnetic order is consistent with Hartree-Fock mean-field theory [55] and saturates to unity in the Heisenberg limit for strong interactions. For any small but nonzero U, the absolute value of $m_{B/C}$ increases with increasing α such that $|m_{B/C}| \sim 0.5$ for $\alpha \to 1$. Such finite local magnetization at B/C sub-lattice for infinitesimal interaction is caused by a flat-band state with constant energy dispersion $E_k \approx 0$ located at the Fermi level. The high spin degeneracy is lifted already by the infinitesimal U, and magnetization develops at the B/C sites that carry the flat band [56]. For $\alpha \to 1$, the local magnetization at sublattice D saturates to unity for infinitesimal U since the D sites get weakly coupled to the rest of the lattice. It is important to note that at $T = 0$ the total magnetization summed over the unit cell is zero for $\alpha \in [0\ 1)$ and finite U although the absolute value of magnetization at different sites is different. For $\alpha = 1$, sublattice D gets isolated from the rest of the lattice showing zero local magnetization for any finite U and we get a ferromagnetic ground state which

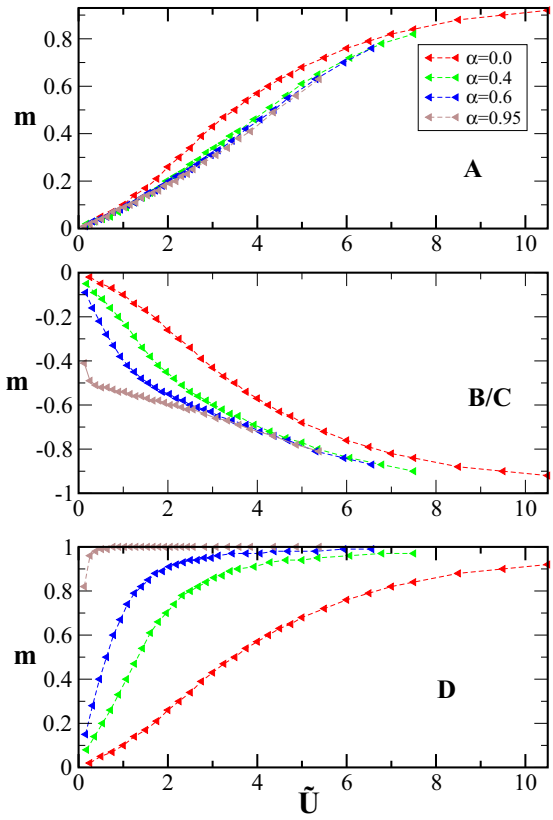

FIG. 2. Magnetic order parameter m for A site (upper panel), B and C sites (middle panel), and D site (lower panel) for varying $\tilde{U}$ and different inhomogeneity α at zero temperature. The Hubbard interaction U has been scaled by $t_+ = (1 + \alpha)t$.

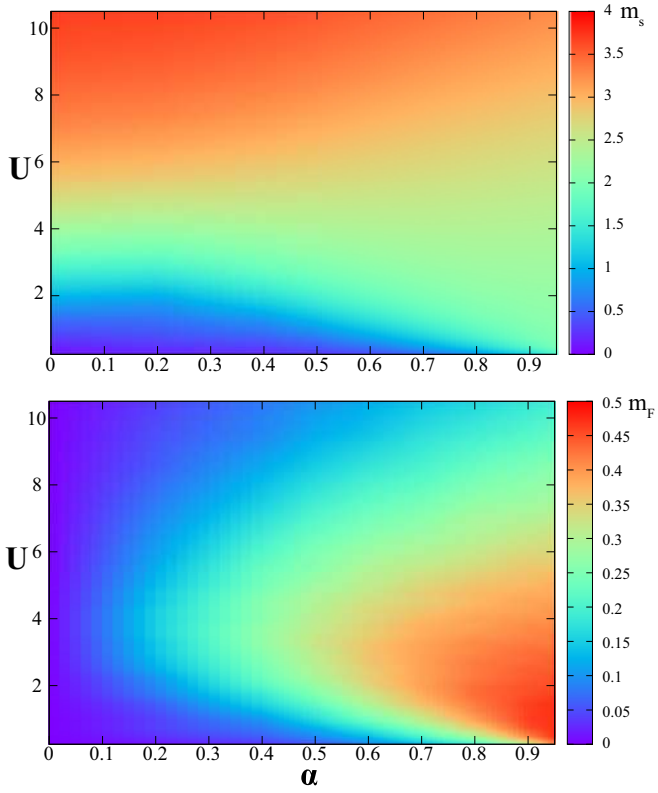

FIG. 3. Upper panel: phase diagram of the inhomogeneous Hubbard model showing staggered magnetization m_s for different inhomogeneity parameter α and interaction U. Lower panel: uniform magnetization for the set of α and U. Here, $m_{\rm F}$ is maximal for $\alpha \to 1$ and $U \to 0$.

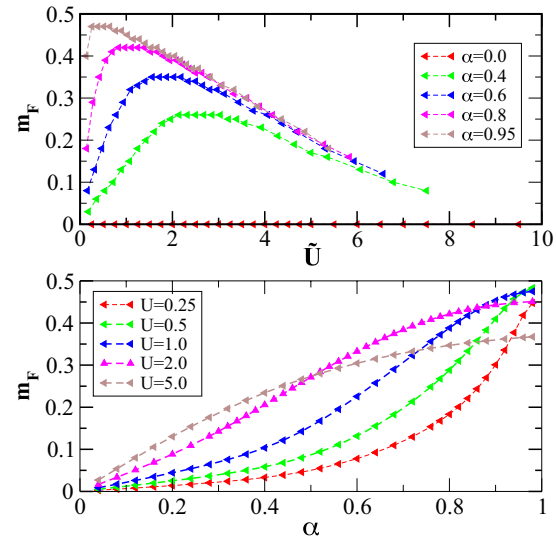

FIG. 4. Upper panel: uniform magnetization $m_{\rm F}$ for varying $\tilde{U}$ and different α. Lower panel: $m_{\rm F}$ for varying α for different U.

is consistent with the Lieb theorem [1]. At finite temperature, thermal fluctuation suppresses the local magnetic order of the weakly coupled sublattice D giving rise to a nonzero total magnetization summed over the unit cell also for $\alpha \to 1$. For the weakly interacting regime, the behavior of $m_{B/C}$ vs $\tilde{U}$ changes from exponential to linear for $\alpha \sim 1$ due to the flat band [56]. Linear behavior of the order parameter with the Hubbard interaction in the weakly interacting regime can be explained with a simple mean-field gap equation with a δ-function density of states [57]. Local magnetizations for all sites coalesce to single curves for all values of α in the strong coupling regime, where the fermions are completely localized so that the system can be described by an effective Heisenberg model and the lattice geometry is insignificant to the behavior of local magnetic order.

In the upper panel of Fig. 3, we show the phase diagram for staggered magnetization, i.e., $m_s = m_A + m_D - 2\, m_{B/C}$, obtained using ED+RDMFT for varying interaction U and inhomogeneity $0 \leqslant \alpha < 1$. For smaller interactions, e.g., $U < 2$, staggered magnetization assumes a finite value for moderate inhomogeneity such that $m_s \sim 2$ for $U \to 0^+$ and $\alpha \to 1$. In the strong coupling Heisenberg limit, absolute value of the local magnetization at different sublattices asymptotically goes to unity for all inhomogeneities and thus $m_s \approx 4$, as evident from Fig. 2. In order to understand the effect of inhomogeneity on spatial distribution of the magnetic order, we show the behavior of uniform magnetization, i.e., $m_F = -(m_{B/C} + m_A)$, in the lower panel of Fig. 3. The uniform magnetization m_F is zero for the homogeneous system for any finite interactions. Also m_F is zero and independent of α in the strongly interacting regimes. However, it gets finite for moderate α and finite but moderate values of U. It has maximum value for $\alpha \to 1$ and $U \to 0^+$. We also show m_F vs $\tilde{U}$ for a set of α values in the upper panel of Fig. 4. For finite α, m_F increases initially with increasing $\tilde{U}$, peaks at a given $\tilde{U}_p(\alpha)$, and then decreases with increasing $\tilde{U}$. The $\tilde{U}_p(\alpha)$ shifts to lower $\tilde{U}$ with increasing α, and $\tilde{U}_p(\alpha) \to 0$ for $\alpha \to 1$. In the strong coupling regime, the $m_F(\tilde{U})$ vs $\tilde{U}$ curves merge together for all values of the inhomogeneity and approach zero asymptotically. Further, we show the uniform magnetization m_F for varying inhomogeneity at different Hubbard interactions in the lower panel of Fig. 4. Below a given interaction strength, m_F increases with increasing α, but the uniform magnetization curve goes to an inflection point. The inflection point shifts to higher α with decreasing U. The inflection in the curve appears at $\alpha \to 1$ in the limit $U \to 0$, indicating a sharp crossover to ferromagnetic state in the Lieb-lattice limit. Such magnetic behavior can be assigned to the flat-band ferromagnetism. For the Lieb-lattice limit ($\alpha \to 1$), B and C sublattices (sites with flat bands) are polarized, with vanishing magnetization at A sublattice, for infinitesimal strength of the interaction. Above the crossover interaction strength the curvature of staggered magnetization is positive and the magnetic behavior is determined by local interactions mainly. Emergence of such uniform magnetization is detrimental to the singlet $d_{x^2-y^2}$ pairing superconductivity defined in Eq. (12). We will discuss the influence of the inhomogeneity on the superconducting order in Sec. III D.

B. Double occupancy

In this section, we study the interplay of the inhomogeneity and the Hubbard interaction in double occupancy at a given site, i.e., $\langle \hat{n}_\uparrow \hat{n}_\downarrow \rangle$ using RDMFT+CT-INT. Double occupancy

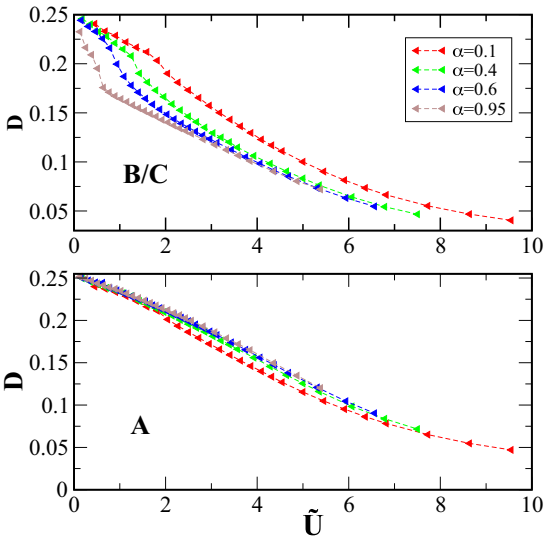

FIG. 5. Upper panel: double occupancy of B/C sites for varying interaction $\tilde{U}$ and different α at $\beta = 1/T = 20$. Lower panel: double occupancy of A sites.

can be a direct measure of local moment formation $\langle m_z^2 \rangle = \langle (\hat{n}_\uparrow - \hat{n}_\downarrow)^2 \rangle = \langle (\hat{n}_\uparrow + \hat{n}_\downarrow - 2\,\hat{n}_\uparrow \hat{n}_\downarrow) \rangle = n - 2\,\langle \hat{n}_\uparrow \hat{n}_\downarrow \rangle$. In the noninteracting limit, the up and down electrons are decoupled, $\langle \hat{n}_\uparrow \hat{n}_\downarrow \rangle = \langle \hat{n}_\uparrow \rangle \langle \hat{n}_\downarrow \rangle$. In Fig. 5, we compare the spatially resolved double occupancy for different inhomogeneities α at small finite temperature $\beta = 1/T = 20$. The double occupancy of the B/C sites is shown in the upper panel and that of the site A is shown in the lower panel. At B/C sites the double occupancy sharply decreases with increasing α for moderate values of $\tilde{U}$. The presence of a flat band favors single occupancy even for infinitesimal interactions as indicated by the sharp decrease of the double occupancy. Kink in the double-occupancy variation corresponds to the critical interaction U_c for the magnetic transition at given temperature. $U_c \to 0^+$ for Lieb-lattice limit at zero temperature [6,56]. The double occupancy $D_{B/C} \to 0.1875$ for $\alpha \to 1$, $U \to 0^+$, and $T \to 0$. This limiting case can be explained as follows. The local magnetization at the B/C sites at $T = 0$ and $U \to 0^+$ is 0.5 for the Lieb lattice at half-filling, i.e., the average number of particles per site is one [6], and thus we can write

$$n_{B/C\uparrow} + n_{B/C\downarrow} = 1.0;\; n_{B/C\uparrow} - n_{B/C\downarrow} = 0.5, \tag{13}$$

giving $\langle \hat{n}_{B/C\uparrow} \rangle = n_{B/C\uparrow} = 0.75$ and $\langle \hat{n}_{B/C\downarrow} \rangle = n_{B/C\downarrow} = 0.25$, and thus $D_{B/C} = \langle \hat{n}_{B/C\uparrow} \rangle \langle \hat{n}_{B/C\downarrow} \rangle = 0.1875$ in the $U \to 0^+$ and $T \to 0$ limits. In the strong coupling limit, for large $\tilde{U}$, double occupancy for different inhomogeneities coalesces and goes to zero asymptotically. At site A the double occupancy coalesces to a single decreasing curve with varying $\tilde{U}$ for moderate to large inhomogeneity.

C. Non-Fermi-liquid behavior

We explore the effect of inhomogeneity on quasiparticle behavior in the weak coupling regime in the nonmagnetic region at small finite temperatures using RDMFT+CT-INT. We find breakdown of the usual Fermi-liquid behavior occurs beyond a critical strength of the inhomogeneity, which is evident from the scattering rate, i.e., the imaginary part of the local self-energy, for different sites within the unit cell. There have been a few theoretical proposals for the origin of non-Fermi-liquid behavior linked to the presence of singularities in the dispersion of the noninteracting part of the Hamiltonian [58–62]. Non-Fermi liquids have also been observed within theories which include nonlocal correlations [63,64]. For a well-defined Fermi liquid, the self-energy for low Matsubara frequencies ω_n can be written as

$$\Sigma(i\omega_n) \approx i\omega_n a + b, \tag{14}$$

where a and b are real constants. The quasiparticle weight $Z = m/m*$, where m is the bare mass and $m*$ is the mass in the presence of many-body effects, can be defined in terms of the self-energy as

$$Z = \left(1 - \frac{\partial \mathrm{Im}\Sigma(i\omega_n)}{\partial \omega_n}\bigg|_{n=0;\; T\to 0}\right)^{-1} \tag{15}$$

and $0 < Z < 1$ for the Fermi liquid. We observe the imaginary part of the self-energy at the lowest numerically calculated Matsubara frequency ω_0 and at the next consecutive frequency ω_1 and define ($a = |\mathrm{Im}\Sigma(i\omega_0)| - |\mathrm{Im}\Sigma(i\omega_1)|$) such that $a < 0$ signifies a Fermi liquid while $a > 0$ is characteristic of a non-Fermi liquid. In the upper panel of Fig. 6, we show the imaginary part of the self-energy at B/C for different inhomogeneities. For small to moderate values of the inhomogeneity, the system is a Fermi liquid with $a < 0$ and well-defined quasiparticle weight Z. For large inhomogeneity, say $\alpha = 0.80$, the self-energy for the $B(C)$ sites, which carry the flat band, diverges for small frequencies $|\omega_n|$ and we observe non-Fermi-liquid behavior with $a > 0$ where quasiparticle weight cannot be well defined. In the lower panel of Fig. 6, we show the self-energy for the A site. The quasiparticle weight can be defined for all inhomogeneities since $a < 0$ although it increases with increasing α.

In Fig. 7, we present $\mathrm{Im}\Sigma(i\omega_{n=0})$ which is an estimate of the inverse of the scattering time $\tau^{-1} \approx -\mathrm{Im}\Sigma(i\omega_{n=0})$. For Fermi-liquid behavior (conventional metallic behavior) the inverse of the scattering time, which is proportional to the resistivity, decreases with decreasing temperature. As shown in the main panel of Fig. 7, we find breakdown of Fermi-liquid behavior as $\mathrm{Im}\Sigma_{B/C}(i\omega_{n=0})$ increases with decreasing temperature for $\alpha \to 1$ and finite interaction $U = 2.0$ while $\mathrm{Im}\Sigma_A(i\omega_{n=0})$ decreases with decreasing temperature displaying Fermi-liquid behavior. In the inset of Fig. 7, we show $\mathrm{Im}\Sigma(i\omega_{n=0})$ vs T for moderate strength of the inhomogeneity, say $\alpha = 0.4$. $\mathrm{Im}\Sigma(i\omega_{n=0})$ decreases with decreasing temperature for both B/C and A sites and the system displays Fermi-liquid (FL) behavior. Non-Fermi-liquid (NFL) behavior in the presence of a flat band has been discussed previously for the multiband Hubbard model with repulsive interaction [65,66]. Doping-driven FL to NFL change has been found using DMFT calculations combined with first-principles density functional theory [65,66]. The origin of such NFL behavior was the nearly flat dispersion present in the given material. Also, a multiorbital Hubbard model with orbital-dependent hoppings has been studied in the context of orbital-selective [67] Mott transition, where the origin of NFL behavior is due to the lattice structure. In our study, we have systematically

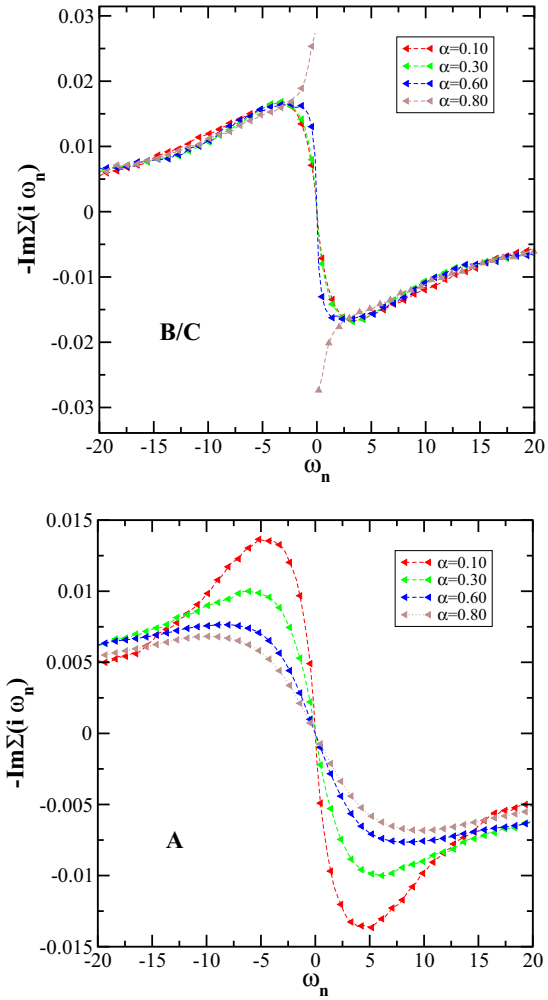

FIG. 6. Upper panel: imaginary part of the local self-energy, i.e., $-\mathrm{Im}\Sigma(i\omega_n)$ vs Matsubara frequency ω_n, for sites B and C, for different α, $T = 0.05$ and $U = 0.75$. For these parameters the system is in the nonmagnetic metallic regime [68]. Lower panel: $-\mathrm{Im}\Sigma(i\omega_n)$ vs Matsubara frequency ω_n, for site A, for the same parameter as upper panel.

tuned the lattice model from dispersive to flat bands to show how the non-Fermi-liquid behavior emerges.

D. Doped Hubbard model

To explore the possible dSC in the presence of finite inhomogeneity away from half-filling, we have carried out cellular DMFT+ED calculations using a 2×2 cluster. Since the present choice of the inhomogeneity expands the unit cell by a factor of 2 in each direction, the four-site plaquette actually comprises a single unit cell of the model. This plaquette DMFT approximation is equivalent to the single-site DMFT for a four-band model in the sense that we get one impurity problem with four spin-degenerate orbitals. We uniformly dope the system by choosing a finite chemical potential μ independent of the lattice site in the unit cell. We allow breaking of the SU(2) spin symmetry and thus long-range antiferromagnetic order. We show the dSC order for different values of chemical potential μ and inhomogeneity α in the

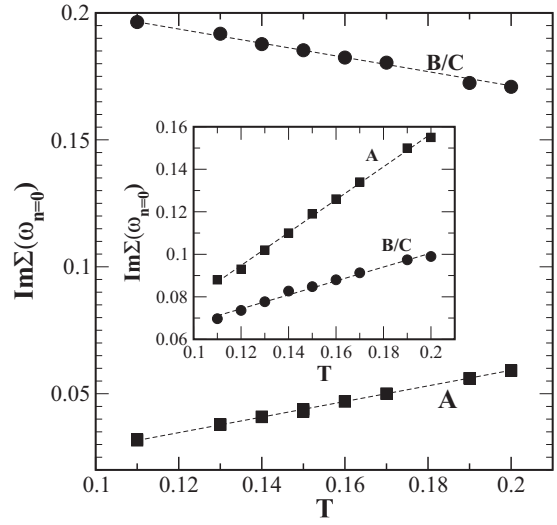

FIG. 7. In the main panel: $\mathrm{Im}\Sigma(i\omega_{n=0})$ vs T at different sites for $\alpha = 0.95$ and $U = 2$. A similar plot is shown for $\alpha = 0.4$ in the inset. For these parameters the system is in the nonmagnetic metallic regime [68].

upper panel of Fig. 8. We observe a region with finite dSC order parameter for moderate inhomogeneity, while dSC is not present for inhomogeneity $\alpha \geqslant 0.4$ for any finite μ. We also observe a region where the dSC order parameter is finite but nonconvergent and oscillates with the DMFT iteration with a period longer than two iteration steps as shown by the circles. We also present the behavior of local magnetization averaged over the unit cell for different μ and α. We obtain a magnetic to nonmagnetic crossover going through a region with magnetic order oscillating with the DMFT iteration in the lower panel of Fig. 8. In this case, such oscillatory solution is observed for $0 < \alpha < 1$ with varying μ.

An example of the DMFT calculations in the region with oscillatory solutions can be seen in Fig. 9. We show the results for two values of the inhomogeneity, i.e., $\alpha = 0.05$ in the upper panel and $\alpha = 0.5$ in the lower panel. For $\alpha = 0.05$, the different order parameters such as dSC, magnetic and density order oscillate with the DMFT iteration with a period longer than two and a convergent solution cannot be achieved. Motivated by the observations in doped 2D homogeneous Hubbard model [69–72], such a behavior has been interpreted as indication that an incommensurate spin density wave is the proper state [73,74] and consequently calculations do not converge in this parameter region. Although there is no direct mathematical foundation for such an interpretation, we have previously reported presence of spatially nonuniform magnetic and charge order coexisting with dSC using an extended plaquette DMFT approximation for the canonical 2D Hubbard model. In that case, calculations were carried out for unit cells with a large number of sites by taking one-dimensional slices of the lattice [27]. There, incommensurate orders coexisting with dSC were reported, such as the spin-density wave (SDW) coexisting with inhomogeneous dSC of wavelength 12 plaquettes which was found to have the lowest energy for $\mu = 1.40$ and $U = 6.0$. Such spatially nonuniform SDW orders reported in several recent works [29,30,74] brace the interpretation. The oscillatory solutions obtained using DMFT

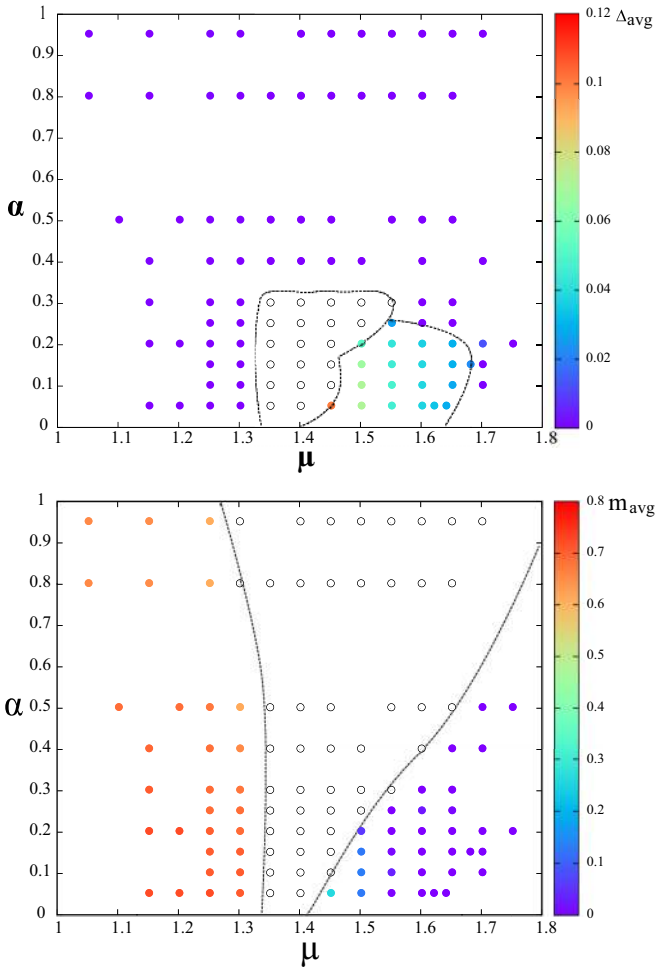

FIG. 8. Upper panel: average dSC order parameter for set of inhomogeneity α and chemical potential μ for the two-dimensional Hubbard model on the inhomogeneous square lattice with modulated hopping at $U = 6.0$. The circles are the data points where we have carried out the plaquette DMFT+ED calculations. The dashed lines are guides to the eye separating different regions. The lines are only qualitative and do not actually correspond to a phase boundary. For solid circles, we obtain a converged DMFT solution while open white circles represent the data set for which DMFT solutions are finite and oscillatory. The color code assigned to the solid circles represents the magnitude of the dSC order parameter. Lower panel: averaged magnetic order as a function of inhomogeneity α and chemical potential μ.

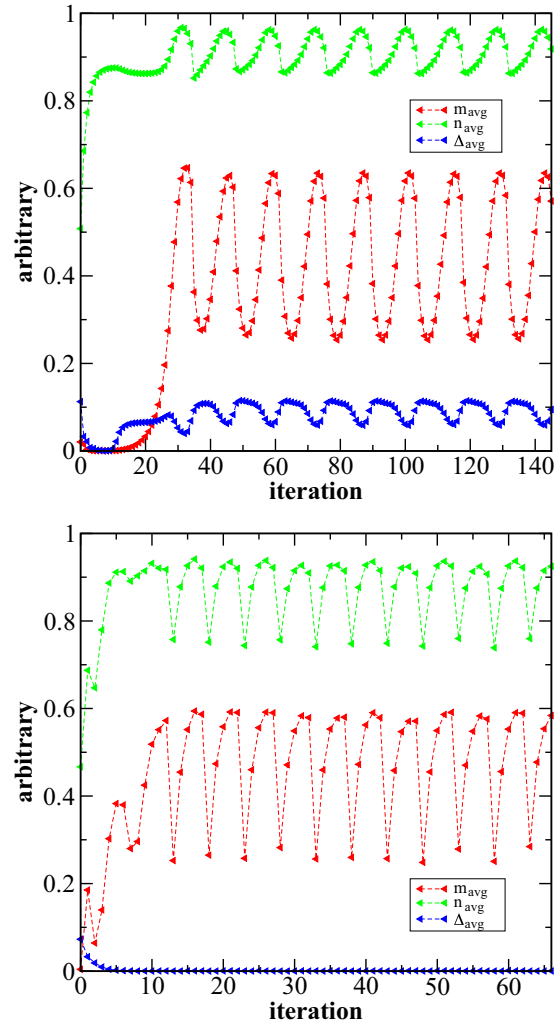

FIG. 9. Upper panel: the order parameters m_{avg}, n_{avg}, and Δ_{avg} for varying DMFT iterations for $\alpha = 0.05$. All quantities show oscillatory behavior. Lower panel: same order parameters for varying DMFT iterations for $\alpha = 0.5$. Here, m_{avg} and n_{avg} oscillate with the DMFT iteration, while Δ_{avg} converges to zero.

can be made to converge using different mixing techniques, but this is likely to lead to a metastable solution given that a long-wavelength SDW is not allowed for the simple plaquette DMFT approximation. For moderate inhomogeneity $\alpha = 0.5$ shown in the lower panel of Fig. 9, we observe the oscillations only for the magnetic and density orders while the superconducting order converges to $\Delta_{\text{avg}} = 0$. This behavior prevails for moderate to large inhomogeneity. It is also possible that other types of orders such as phase separation could exist in the region where nonconvergent solutions are found [75]. A typical sign for phase separation is a first-order jump in the density with tuning μ [73], and such sensitivity to μ is also associated with the region of oscillatory solutions.

The results for the uniform dSC order parameter corresponding to converged DMFT solutions, for several values of inhomogeneity α displayed in Fig. 10, exhibit interesting features. We find that the strength of dSC decreases monotonically as a function of α over the entire doping range. Our findings complement the results of previous studies of interplay of lattice inhomogeneity and interactions in the context of dSC on the checkerboard lattice using CDMFT [42]. CDMFT calculations show a monotonic decrease in the dSC order with inhomogeneity, i.e., the ratio of the interplaquette to intraplaquette hopping. Dynamical cluster approximation (DCA) finds monotonic decrease of the critical temperature with strength of the inhomogeneity [41]. In contrast, DQMC calculations for similar inhomogeneity pattern find an optimal value for which the pair vertex is most attractive [40]. In both approaches, the dSC order eventually vanishes for large inhomogeneity. In this study, dSC is completely destroyed for $\alpha \geqslant 0.25$. A few other patterns of inhomogeneity where an onsite potential of one fourth of the lattice sites of the

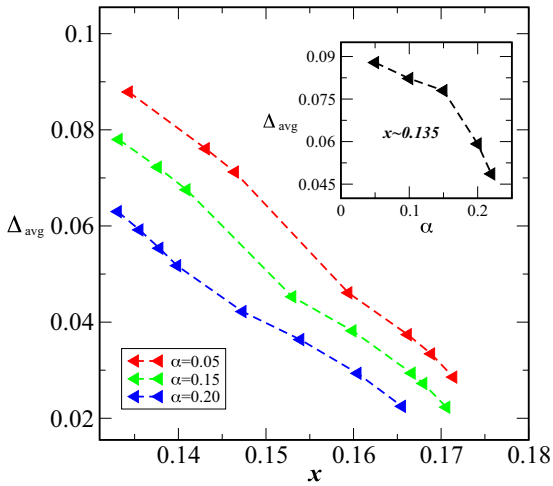

FIG. 10. Main panel: uniform dSC order parameter for converged DMFT solutions Δ_{avg} vs doping x for different values of α and $U = 6.0$ at $T = 0$. Uniform dSC order monotonically decreases with increasing x. Magnitude of dSC is smaller for larger inhomogeneity at given x and is zero for $\alpha \geqslant 0.25$. In the inset: uniform dSC order parameter for varying α for given $x = 0.135$.

square lattice is raised by an amount V_0 such that in the limit $V_0 \to \infty$, the lattice maps onto the "Lieb-lattice" Hamiltonian have been studied [40]. It has been found that this kind of inhomogeneity rapidly, and monotonically, suppresses the dSC pairing.

IV. CONCLUSIONS

To understand the spatial nonuniformity of the various order parameters in systems ranging from real materials to cold atom systems, Hubbard Hamiltonians with different inhomogeneity patterns have been proposed. The pattern of inhomogeneity explored in this work leads to the Lieb-lattice geometry as a limiting case. Importantly, this allows the study of the effect of an emerging flat-band singularity. We have applied RDMFT to explore the influence of inhomogeneity on different physical properties at half-filling and finite Hubbard interactions. The inhomogeneity changes the magnetic behavior of the system, interpolating between the square-lattice and Lieb-lattice cases. Below a given interaction strength, the uniform magnetization displays a sharp crossover to a ferromagnetic state with increasing the inhomogeneity. There is an associated inflection point in the uniform magnetization vs the inhomogeneity parameter, with the sharp crossover. Such a behavior is due to a flat-band dispersion appearing when tuning of the inhomogeneity. We also observe a breakdown of Fermi-liquid behavior when the inhomogeneity is increased, signaled by the inverse scattering time defined by the local self-energy.

To capture the nonlocal d-wave superconductor (dSC) order parameter away from half-filling, we employ cellular dynamical mean-field theory (CDMFT) combined with an ED impurity solver for a cluster of four sites (2×2). For a range of doping values we observe oscillatory behavior in the DMFT iteration, which we tentatively associate with incommensurate spin-density-wave order. For small inhomogeneity the system displays uniform dSC and also dSC coexisting with the incommensurate order depending on the chemical potential. We find suppression of the dSC order parameter for moderate to large inhomogeneity, while the oscillatory solutions associated with incommensurate order persist for all finite values of the inhomogeneity. The presence of incommensurate order coexisting with dSC in the homogeneous case is in accordance with recent findings [27,76], although further work would be needed to determine the actual wavelength and other properties of the spin-density wave.

Our findings can be relevant to ultracold gas experiments, where the simple two-dimensional Hubbard model [77–83] as well as different inhomogeneity patterns and lattice geometries [78,84–86] have been realized. Experimentally, the geometry of an optical lattice can be determined by the spatial arrangement of the laser beams, and the tunneling of the trapped atoms within the lattice is then tuned via the laser amplitudes [87]. Spin correlations displaying antiferromagnetic behavior have been observed using Bragg scattering [88] and fermionic microscopes [89,90]. Using these techniques, it could be possible to also study magnetism in optical Lieb lattices populated with fermionic atoms [19,22]. Our results show how an imperfect, quasiflat band affects the double occupancy and magnetization, and could thus aid interpretation of such experimental results. It could also be possible to experimentally engineer the exact model that we have proposed here. A square-to-Lieb-lattice crossover could be studied by tuning the laser amplitudes in the configuration used in previous experiments [20], although the corresponding tight-binding lattice will also include onsite potential contributions on the D sites. Nevertheless, this is perhaps the easiest way to study a tunable flat band within ultracold gas systems.

ACKNOWLEDGMENTS

This work was supported by the Academy of Finland through its Centers of Excellence Programme (2012-2017) and under Projects No. 284621, No. 303351, and No. 307419, by the European Research Council under Grants No. ERC-2013-AdG-340748-CODE and No. ERC-2017-COG-771891-QSIMCORR, and by the Deutsche Forschungsgemeinschaft (DFG, German Research Foundation) under Germanys Excellence Strategy Grant No. EXC-2111 390814868. T.I.V. acknowledges support from the Alexander von Humboldt foundation. Computing resources were provided by CSC, the Finnish IT Centre for Science.

[1] E. H. Lieb, Phys. Rev. Lett. **62**, 1201 (1989).
[2] H. Tasaki, Phys. Rev. Lett. **69**, 1608 (1992).
[3] A. Mielke and H. Tasaki, Commun. Math. Phys. **158**, 341 (1993).

[4] H. Tasaki, Prog. Theor. Phys. **99**, 489 (1998).
[5] R. Arita, Y. Suwa, K. Kuroki, and H. Aoki, Phys. Rev. Lett. **88**, 127202 (2002).
[6] K. Noda, A. Koga, N. Kawakami, and T. Pruschke, Phys. Rev. A **80**, 063622 (2009).
[7] K. Noda, K. Inaba, and M. Yamashita, Phys. Rev. A **90**, 043624 (2014).
[8] N. Hartman, W.-T. Chiu, and R. T. Scalettar, Phys. Rev. B **93**, 235143 (2016).
[9] N. C. Costa, T. Mendes-Santos, T. Paiva, R. R. dos Santos, and R. T. Scalettar, Phys. Rev. B **94**, 155107 (2016).
[10] V. A. Khodel' and V. R. Shaginyan, Pis'ma Zh. Eksp. Teor. Fiz. **51**, 488 (1990) [JETP Lett. **51**, 553 (1990)].
[11] N. B. Kopnin, T. T. Heikkilä, and G. E. Volovik, Phys. Rev. B **83**, 220503(R) (2011).
[12] V. I. Iglovikov, F. Hébert, B. Grémaud, G. G. Batrouni, and R. T. Scalettar, Phys. Rev. B **90**, 094506 (2014).
[13] S. Peotta and P. Törmä, Nat. Commun. **6**, 8944 (2015).
[14] Y. Cao, V. Fatemi, A. Demir, S. Fang, S. L. Tomarken, J. Y. Luo, J. D. Sanchez-Yamagishi, K. Watanabe, T. Taniguchi, E. Kaxiras, R. C. Ashoori, and P. Jarillo-Herrero, Nature (London) **556**, 80 (2018).
[15] Y. Cao, V. Fatemi, S. Fang, K. Watanabe, T. Taniguchi, E. Kaxiras, and P. Jarillo-Herrero, Nature (London) **556**, 43 (2018).
[16] M. Yankowitz, S. Chen, H. Polshyn, Y. Zhang, K. Watanabe, T. Taniguchi, D. Graf, A. F. Young, and C. R. Dean, Science **363**, 1059 (2019).
[17] M. R. Slot, T. S. Gardenier, P. H. Jacobse, G. C. P. van Miert, S. N. Kempkes, S. J. M. Zevenhuizen, C. M. Smith, D. Vanmaekelbergh, and I. Swart, Nat. Phys. **13**, 672 (2017).
[18] R. Drost, T. Ojanen, A. Harju, and P. Liljeroth, Nat. Phys. **13**, 668 (2017).
[19] D. Leykam, A. Andreanov, and S. Flach, Adv. Phys. **3**, 1473052 (2018).
[20] S. Taie, H. Ozawa, T. Ichinose, T. Nishio, S. Nakajima, and Y. Takahashi, Sci. Adv. **1**, e1500854 (2015).
[21] H. Ozawa, S. Taie, T. Ichinose, and Y. Takahashi, Phys. Rev. Lett. **118**, 175301 (2017).
[22] S. Taie, T. Ichinose, H. Ozawa, and Y. Takahashi, arXiv:1708.01100.
[23] R. Bistritzer and A. H. MacDonald, Proc. Natl. Acad. Sci. USA **108**, 12233 (2011).
[24] E. W. Huang, M.-S. Vaezi, Z. Nussinov, and A. Vaezi, Phys. Rev. B **99**, 235128 (2019).
[25] S. Sayyad, E. W. Huang, M. Kitatani, M.-S. Vaezi, Z. Nussinov, A. Vaezi, and H. Aoki, arXiv:1903.09888.
[26] H.-M. Guo, L. Wang, and R. T. Scalettar, Phys. Rev. B **97**, 235152 (2018).
[27] T. I. Vanhala and P. Törmä, Phys. Rev. B **97**, 075112 (2018).
[28] B. Keimer, S. A. Kivelson, M. R. Norman, S. Uchida, and J. Zaanen, Nature (London) **518**, 179 (2015).
[29] B.-X. Zheng, C.-M. Chung, P. Corboz, G. Ehlers, M.-P. Qin, R. M. Noack, H. Shi, S. R. White, S. Zhang, and G. K.-L. Chan, Science **358**, 1155 (2017).
[30] G. Salomon, J. Koepsell, J. Vijayan, T. A. Hilker, J. Nespolo, L. Pollet, I. Bloch, and C. Gross, Nature (London) **565**, 56 (2019).
[31] D. Shechtman, I. Blech, D. Gratias, and J. W. Cahn, Phys. Rev. Lett. **53**, 1951 (1984).
[32] I. Bloch, J. Dalibard, and W. Zwerger, Rev. Mod. Phys. **80**, 885 (2008).
[33] J. González, F. Guinea, and M. A. H. Vozmediano, Phys. Rev. B **59**, R2474 (1999).
[34] A. Ohtomo, D. A. Muller, J. L. Grazul, and H. Y. Hwang, Nature (London) **419**, 378 (2002).
[35] M. Hohenadler and F. F. Assaad, J. Phys.: Condens. Matter **25**, 143201 (2013).
[36] P. Kumar, T. Mertz, and W. Hofstetter, Phys. Rev. B **94**, 115161 (2016).
[37] E. Fradkin and S. A. Kivelson, Nat. Phys. **8**, 864 (2012).
[38] M.-H. Julien, Science **350**, 914 (2015).
[39] S. Okamoto and T. A. Maier, Phys. Rev. B **81**, 214525 (2010).
[40] T. Ying, R. Mondaini, X. D. Sun, T. Paiva, R. M. Fye, and R. T. Scalettar, Phys. Rev. B **90**, 075121 (2014).
[41] D. G. S. P. Doluweera, A. Macridin, T. A. Maier, M. Jarrell, and T. Pruschke, Phys. Rev. B **78**, 020504(R) (2008).
[42] S. Chakraborty, D. Sénéchal, and A.-M. S. Tremblay, Phys. Rev. B **84**, 054545 (2011).
[43] W.-F. Tsai, H. Yao, A. Läuchli, and S. A. Kivelson, Phys. Rev. B **77**, 214502 (2008).
[44] Y. Wu, S. Fang, G. Liu, and Y. Zhang, J. Phys.: Condens. Matter **31**, 375601 (2019).
[45] P. M. Smith and M. P. Kennett, Phys. Rev. B **88**, 214518 (2013).
[46] H. Yao, W.-F. Tsai, and S. A. Kivelson, Phys. Rev. B **76**, 161104(R) (2007).
[47] M. Snoek, I. Titvinidze, C. Töke, K. Byczuk, and W. Hofstetter, New J. Phys. **10**, 093008 (2008).
[48] M. O. J. Heikkinen, D.-H. Kim, M. Troyer, and P. Törmä, Phys. Rev. Lett. **113**, 185301 (2014).
[49] A. Georges, G. Kotliar, W. Krauth, and M. J. Rozenberg, Rev. Mod. Phys. **68**, 13 (1996).
[50] F. F. Assaad and T. C. Lang, Phys. Rev. B **76**, 035116 (2007).
[51] R. Jordens, N. Strohmaier, K. Gunter, H. Moritz, and T. Esslinger, Nature (London) **455**, 204 (2008).
[52] T. Maier, M. Jarrell, T. Pruschke, and M. H. Hettler, Rev. Mod. Phys. **77**, 1027 (2005).
[53] A. I. Lichtenstein and M. I. Katsnelson, Phys. Rev. B **62**, R9283 (2000).
[54] M. Capone and G. Kotliar, Phys. Rev. B **74**, 054513 (2006).
[55] J. E. Hirsch, Phys. Rev. B **31**, 4403 (1985).
[56] P. Kumar, T. I. Vanhala, and P. Törmä, Phys. Rev. B **96**, 245127 (2017).
[57] K. Noda, K. Inaba, and M. Yamashita, Phys. Rev. A **91**, 063610 (2015).
[58] C. M. Varma, P. B. Littlewood, S. Schmitt-Rink, E. Abrahams, and A. E. Ruckenstein, Phys. Rev. Lett. **63**, 1996 (1989).
[59] S. Gopalan, O. Gunnarsson, and O. K. Andersen, Phys. Rev. B **46**, 11798 (1992).
[60] R. Hlubina and T. M. Rice, Phys. Rev. B **51**, 9253 (1995).
[61] Igor Dzyaloshinskii, J. Phys. I (France) **6**, 119 (1996).
[62] A. A. Katanin and A. P. Kampf, Phys. Rev. B **68**, 195101 (2003).
[63] A. N. Rubtsov, M. I. Katsnelson, A. I. Lichtenstein, and A. Georges, Phys. Rev. B **79**, 045133 (2009).
[64] A. Liebsch and N.-H. Tong, Phys. Rev. B **80**, 165126 (2009).
[65] H. Shinaoka, S. Hoshino, M. Troyer, and P. Werner, Phys. Rev. Lett. **115**, 156401 (2015).

[66] A. Hausoel, M. Karolak, E. Sasioglu, A. Lichtenstein, K. Held, A. Katanin, A. Toschi, and G. Sangiovanni, Nat. Commun. **8**, 16062 (2017).
[67] M. Ferrero, F. Becca, M. Fabrizio, and M. Capone, Phys. Rev. B **72**, 205126 (2005).
[68] E. Miranda and V. Dobrosavljevi, Rep. Prog. Phys. **68**, 2337 (2005).
[69] E. Arrigoni and G. C. Strinati, Phys. Rev. B **44**, 7455 (1991).
[70] J. K. Freericks and M. Jarrell, Phys. Rev. Lett. **74**, 186 (1995).
[71] M. Fleck, A. I. Liechtenstein, A. M. Oleś, L. Hedin, and V. I. Anisimov, Phys. Rev. Lett. **80**, 2393 (1998).
[72] M. Fleck, A. I. Lichtenstein, A. M. Oleś, and L. Hedin, Phys. Rev. B **60**, 5224 (1999).
[73] R. Peters and T. Pruschke, New J. Phys. **11**, 083022 (2009).
[74] R. Peters and N. Kawakami, Phys. Rev. B **89**, 155134 (2014).
[75] A. Macridin, M. Jarrell, and T. Maier, Phys. Rev. B **74**, 085104 (2006).
[76] A. S. Darmawan, Y. Nomura, Y. Yamaji, and M. Imada, Phys. Rev. B **98**, 205132 (2018).
[77] J. F. Sherson, C. Weitenberg, M. Endres, M. Cheneau, I. Bloch, and S. Kuhr, Nature (London) **467**, 68 (2010).
[78] L. Tarruell, D. Greif, T. Uehlinger, G. Jotzu, and T. Esslinger, Nature (London) **483**, 302 (2012).
[79] D. Greif, M. F. Parsons, A. Mazurenko, C. S. Chiu, S. Blatt, F. Huber, G. Ji, and M. Greiner, Science **351**, 953 (2016).
[80] L. W. Cheuk, M. A. Nichols, K. R. Lawrence, M. Okan, H. Zhang, E. Khatami, N. Trivedi, T. Paiva, M. Rigol, and M. W. Zwierlein, Science **353**, 1260 (2016).
[81] L. W. Cheuk, M. A. Nichols, K. R. Lawrence, M. Okan, H. Zhang, and M. W. Zwierlein, Phys. Rev. Lett. **116**, 235301 (2016).
[82] E. Cocchi, L. A. Miller, J. H. Drewes, M. Koschorreck, D. Pertot, F. Brennecke, and M. Köhl, Phys. Rev. Lett. **116**, 175301 (2016).
[83] P. T. Brown, D. Mitra, E. Guardado-Sanchez, P. Schauß, S. S. Kondov, E. Khatami, T. Paiva, N. Trivedi, D. A. Huse, and W. S. Bakr, Science **357**, 1385 (2017).
[84] J. Struck, C. Ölschläger, R. Le Targat, P. Soltan-Panahi, A. Eckardt, M. Lewenstein, P. Windpassinger, and K. Sengstock, Science **333**, 996 (2011).
[85] M. Messer, R. Desbuquois, T. Uehlinger, G. Jotzu, S. Huber, D. Greif, and T. Esslinger, Phys. Rev. Lett. **115**, 115303 (2015).
[86] K. Loida, J.-S. Bernier, R. Citro, E. Orignac, and C. Kollath, Phys. Rev. Lett. **119**, 230403 (2017).
[87] T. Esslinger, Annu. Rev. Condens. Matter Phys. **1**, 129 (2010).
[88] R. A. Hart, P. M. Duarte, T.-L. Yang, X. Liu, T. Paiva, E. Khatami, R. T. Scalettar, N. Trivedi, D. A. Huse, and R. G. Hulet, Nature (London) **519**, 211 (2015).
[89] M. F. Parsons, A. Mazurenko, C. S. Chiu, G. Ji, D. Greif, and M. Greiner, Science **353**, 1253 (2016).
[90] A. Mazurenko, C. S. Chiu, G. Ji, M. F. Parsons, M. Kanász-Nagy, R. Schmidt, F. Grusdt, E. Demler, D. Greif, and M. Greiner, Nature (London) **545**, 462 (2017).